# Paraoxonase 3 functions as a chaperone to decrease functional expression of the epithelial sodium channel

Received for publication, November 5, 2019, and in revised form, February 17, 2020 Published, Papers in Press, February 20, 2020, DOI 10.1074/jbc.RA119.011789

**Shujie Shi[‡1], Nicolas Montalbetti[‡], Xueqi Wang (王雪琪)[‡§], Brittney M. Rush[‡], Allison L. Marciszyn[‡], Catherine J. Baty[‡], Roderick J. Tan[‡], Marcelo D. Carattino[‡¶], and Thomas R. Kleyman[‡¶‖]**

*From the [‡]Renal-Electrolyte Division, Department of Medicine and Departments of [¶]Cell Biology and [‖]Pharmacology and Chemical Biology, University of Pittsburgh, Pittsburgh, Pennsylvania 15261 and [§]Department of Nephrology, Second Xiangya Hospital of Central South University, Changsha 410011, Hunan, China*

Edited by Mike Shipston

**The paraoxonase (PON) family comprises three highly conserved members: PON1, PON2, and PON3. They are orthologs of *Caenorhabditis elegans* MEC-6, an endoplasmic reticulum–resident chaperone that has a critical role in proper assembly and surface expression of the touch-sensing degenerin channel in nematodes. We have shown recently that MEC-6 and PON2 negatively regulate functional expression of the epithelial $Na^+$ channel (ENaC), suggesting that the chaperone function is conserved within this family. We hypothesized that other PON family members also modulate ion channel expression. Pon3 is specifically expressed in the aldosterone-sensitive distal tubules in the mouse kidney. We found here that knocking down endogenous Pon3 in mouse cortical collecting duct cells enhanced $Na^+$ transport, which was associated with increased γENaC abundance. We further examined Pon3 regulation of ENaC in two heterologous expression systems, Fisher rat thyroid cells and *Xenopus* oocytes. Pon3 coimmunoprecipitated with each of the three ENaC subunits in Fisher rat thyroid cells. As a result of this interaction, the whole-cell and surface abundance of ENaC α and γ subunits was reduced by Pon3. When expressed in oocytes, Pon3 inhibited ENaC-mediated amiloride-sensitive $Na^+$ currents, in part by reducing the surface expression of ENaC. In contrast, Pon3 did not alter the response of ENaC to chymotrypsin-mediated proteolytic activation or [2-(trimethylammonium)ethyl]methanethiosulfonate–induced activation of $\alpha\beta_{S518C}\gamma$, suggesting that Pon3 does not affect channel open probability. Together, our results suggest that PON3 regulates ENaC expression by inhibiting its biogenesis and/or trafficking.**

The epithelial $Na^+$ channel (ENaC)[2] mediates the rate-limiting step of $Na^+$ uptake across the apical membrane of epithelia, including kidney tubules, alveoli, and distal colon (1–3). ENaC-dependent $Na^+$ reabsorption in the kidney is essential for regulating extracellular fluid volume and blood pressure (BP) as well as extracellular $[K^+]$ (4–8). ENaC-dependent $Na^+$ absorption in the airway has important roles in airway surface liquid volume maintenance and mucociliary clearance (9–12). ENaC gain-of-function mutations, as found in patients with Liddle syndrome, result in $Na^+$ retention, extracellular volume expansion, hypertension, and hypokalemia (13–17). On the other hand, ENaC loss-of-function mutations result in renal $Na^+$ wasting, hypotension, and hyperkalemia (18–20). These changes in extracellular $[K^+]$ will likely impact the activity of the Na–Cl cotransporter (NCC), contributing to changes in BP seen in these disorders (21–24). Therefore, the expression and activity of ENaC need to be tightly regulated by various endogenous and extracellular factors.

The canonical ENaC consists of three homologous subunits: α, β, and γ (25, 26). The fourth ENaC subunit, δ has been identified in multiple tissues of primates and other species (27, 28). ENaC is synthesized in the endoplasmic reticulum, where nascent α, β, and γ subunits are folded and assembled into trimeric channel complexes that are shuttled to the Golgi apparatus for additional processing and then inserted into the plasma membrane (29–33). Misfolded subunits are subjected to endoplasmic reticulum–associated degradation via the proteasome (34–36). When at the cell surface, ENaC can be ubiquitinated by E3 ligases, which promotes channel internalization by clathrin-mediated endocytosis (37, 38). The retrieved channel complex may then be shuttled to the lysosome for degradation or deubiquitinated and recycled back to the cell surface (39). Together, this multistage machinery determines the total number of functional channels at the cell surface. Molecular chaperones have been implicated in multiple key steps during ENaC biogenesis, trafficking, and degradation (34, 40–45), including members of the paraoxonase (PON) family.

There are three highly conserved genes in the mammalian PON family: *PON1*, *PON2*, and *PON3*. Although all three PONs have antioxidative and anti-atherosclerotic properties (46–50), they differ in their tissues expression and substrate

This work was supported, in whole or in part, by NIDDK, National Institutes of Health Grants DK103834 and DK119752 (to S. S.), DK038470 (to T. R. K.), and DK079307 (to the Pittsburgh Center for Kidney Research); NHLBI, National Institutes of Health Grant HL147818 (to T. R. K.); and National Institutes of Health Grant S10OD021627 (to C. J. B). The authors declare that they have no conflicts of interest with the contents of this article. The content is solely the responsibility of the authors and does not necessarily represent the official views of the National Institutes of Health.

[1] To whom correspondence should be addressed: Renal-Electrolyte Division, University of Pittsburgh, 3550 Terrace St., Pittsburgh, PA 15261. Tel.: 412-383-9569; E-mail: shs117@pitt.edu.

[2] The abbreviations used are: ENaC, epithelial $Na^+$ channel; BP, blood pressure; NCC, Na–Cl cotransporter; PON, paraoxonase; KD, knockdown; FRT, Fisher rat thyroid; DCT, distal convoluted tubule; CNT, connecting tubule; CD, collecting duct; PC, principal cell; IC, intercalated cell; V-ATPase, vacuolar $H^+$-ATPase; $I_{sc}$, short circuit current; NC, negative control; γGT, γ-glutamyl transferase; ROMK, renal outer medullary $K^+$ channel; MTSET, [2-(trimethylammonium)ethyl]methanethiosulfonate; ANOVA, analysis of variance; mCCD, mouse cortical collecting duct; $P_O$, open probability.

specificity. PON2 is ubiquitously expressed in various tissues and most major organs, whereas PON1 and PON3 were thought to be mainly synthesized by the liver and circulate within high-density lipoprotein particles (47, 51–53). However, recent studies have detected PON3 in epithelial cells within many tissues, including the digestive tract, respiratory system, reproductive system, and kidneys (54). Although all three PONs possess lactonase activity, only PON1 can hydrolyze organophosphates, such as paraoxon and its derivatives (48, 51). PONs share evolutionary conservation with *Caenorhabditis elegans* MEC-6 and several other predicted proteins in nematodes. MEC-6 is a chaperone protein that is required for proper folding, assembly, and surface expression of the touch-sensitive MEC-4/MEC-10 channel in the nematode's touch receptor neurons (55, 56). We have shown recently that PON2 inhibits ENaC activity by reducing channel surface expression (57), suggesting that the chaperone function is conserved between mammalian PONs and their nematode orthologs.

There is evidence suggesting that mammalian PONs have important roles in kidney function. *Pon1* KO mice were hypotensive with a lower serum aldosterone level (58). Knockdown (KD) of Pon2 by renal subcapsular infusion of *Pon2* siRNA led to hypertension in rats (59). Although it is unclear whether altered ENaC activity and/or expression contribute to the changes in BP in these models, they collectively support a role of PONs in maintaining normal BP. Being the most neglected member of this family, the role of PON3 in BP control has not been investigated in whole-animal studies. However, *Pon3* transcripts have been detected in multiple nephron segments in the rat kidney and in principal cells and intercalated cells of the mouse distal nephron (60, 61). PON3 shares high sequence homology with PON2 (>60%), which led us to hypothesize that PON3 also functions as a chaperone to regulate ENaC expression. This study examined the expression of Pon3 in the mouse kidney and its effect on ENaC functional expression by silencing endogenous *Pon3* in mouse cortical collecting duct cells or overexpressing Pon3 in cultured FRT cells or *Xenopus* oocytes.

## Results

### *Pon3 expression in the mouse kidney*

To determine whether ENaC is an endogenous substrate for PON3, we first asked whether PON3 localizes to the aldosterone-sensitive distal nephron where ENaC resides. Despite the detection of *Pon3* transcripts in multiple nephron segments and cell types in rodents (60, 61), the expression of PON3 protein in the kidney has not been thoroughly investigated. We approached this question with immunofluorescence staining. Kidney sections from WT C57BL/6 mice were incubated with an anti-PON3 antibody and imaged from the cortex to the medulla using a tile scan technique. As shown in the automatically merged tile scans (Fig. 1*A*), Pon3 localizes mainly in tubular epithelial cells within the cortex but is also present in a specific population of cells of the medulla. To further define the tubular expression of Pon3, we performed costaining experiments using specific markers of different nephron segments. As shown in the overlaid images (Fig. 1*B*), Pon3 was absent in tubules showing positive staining of the Na–K–Cl cotransporter or parvalbumin, suggesting that Pon3 is not expressed in the thick ascending limb or the early distal convoluted tubule (DCT1 (62, 63)). In contrast, we detected Pon3 in a subpopulation of NCC-positive tubules, likely to be the late DCT (DCT2, Fig. 1*B*). Of a total of 148 NCC-positive tubules, 91 tubules showed positive staining for Pon3. Within these NCC/Pon3 double-positive tubules, Pon3 was ubiquitously expressed in nearly all NCC-positive cells. As shown in Fig. 1*B*, Pon3 also colocalized with the cytoplasmic $Ca^{2+}$-binding protein calbindin D28K ($CaBP_{28K}$), a marker for distal tubules with higher abundance in the DCT2 and connecting tubule (CNT) and lower expression in the DCT1 and collecting duct (CD) (64, 65). Among 78 distal tubules with strong $CaBP_{28K}$ staining, 90.6% ± 5.3% cells expressed both $CaBP_{28K}$ and Pon3. To further examine in which cell type Pon3 is expressed, WT mouse kidney sections were costained for Pon3 with the principal cell (PC) marker aquaporin 2 (AQP2) or the intercalated cell (IC) marker vacuolar $H^+$-ATPase (V-ATPase) (66, 67). As shown in the merged images in Fig. 1*B*, Pon3 was expressed in both PCs and ICs but with distinctive expression patterns. Nearly all ICs within a total of 97 V-ATPase–positive tubules were also positive for Pon3. Although all AQP2-positive tubules ($n = 115$) exhibited Pon3 staining, only 25.1% ± 8.8% PCs within AQP2/Pon3 double-positive tubules expressed both AQP2 and Pon3. The specificity of the anti-PON3 antibody was validated with kidney sections of *Pon3* KO mice. We did not observe significant Pon3 staining in tubules from KO animals and only weak staining within glomeruli (Fig. 1*C*). Together, our data suggest that Pon3 is primarily expressed in the DCT2, CNT, and CD of the aldosterone-sensitive distal nephron.

### *Pon3 KD in mouse CCD (mCCD) cells enhances ENaC-mediated $Na^+$ transport*

As Pon3 is expressed in principal cells of the distal nephron (Fig. 1*B*), we examined the role of endogenous Pon3 in regulating ENaC expression and function with siRNA-mediated KD. mCCD cells, derived from the mouse cortical CD, express all three ENaC subunits as well as mineralocorticoid and glucocorticoids receptors (68). As expected, endogenous Pon3 was detected as a single band near 40 kDa in mCCD cells (Fig. 2*C*). To knock down Pon3, mCCD cells were transiently transfected with *Pon3*-specific siRNA, and ENaC-mediated $Na^+$ transport was determined with short-circuit current ($I_{sc}$) measurements. As shown in Fig. 2, Pon3 expression in mCCD cells was reduced 55% ± 14% ($n = 11$, $p < 0.001$) compared with negative control (NC) cells transfected with scrambled siRNAs (Fig. 2*D*). As a result, we observed a 1.2 ± 0.2-fold ($n = 12$, $p < 0.01$) increase in amiloride-sensitive $I_{sc}$ in Pon3 KD cells (Fig. 2*B*) without noticeable changes in transepithelial resistance (1.13 ± 0.49 kilo-ohm for Pon3 KD cells *versus* 1.22 ± 0.34 kilo-ohm for NC cells, $n = 12$, $p = 0.62$). The enhanced $Na^+$ transport in Pon3 KD cells was associated with a 1.4 ± 0.4-fold increase in the abundance of cleaved γENaC ($n = 11$, $p < 0.05$). The abundance of uncleaved γENaC was not affected by Pon3 KD (Fig. 2*E*). In addition, the ratio of cleaved *versus* total γENaC was

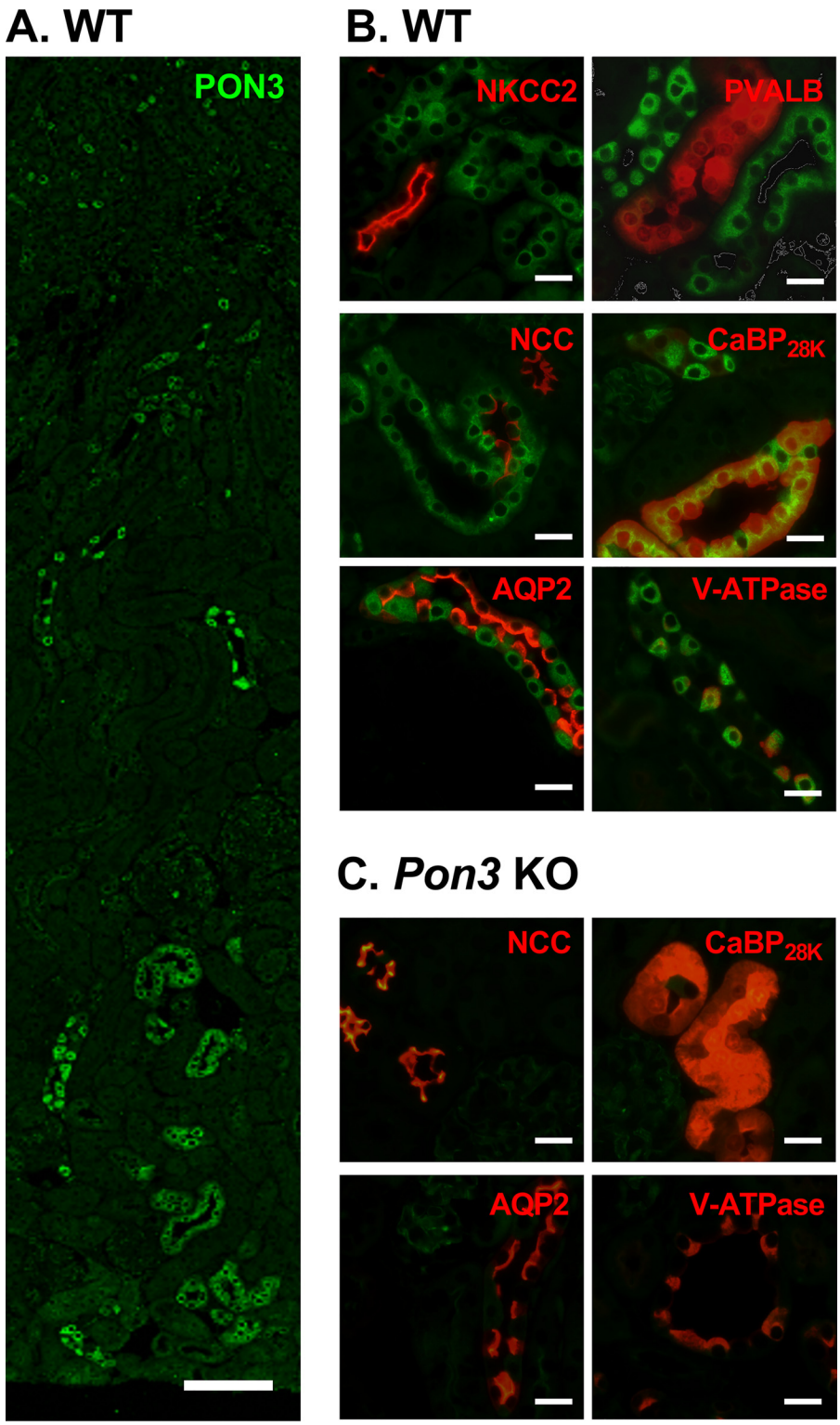


**Figure 1. Nephron segment–specific expression of Pon3 in the mouse kidney.** *A*, transverse-sectioned kidneys of WT C57BL6 mice were stained for PON3 (*green*) and imaged from the cortex to the medulla using a tile scan technique. *Scale bar* = 100 $\mu$m. *B*, merged images of kidney sections costained for PON3 (*green*) and nephron segment–specific markers (*red*) in WT mice: NKCC2, Na-K-Cl cotransporter *PVALB*, parvalbumin. *C*, anti-PON3 antibody specificity was validated in *Pon3* KO mice. Scale bars in *B* and *C* = 20 $\mu$m. Representative images are shown for kidney sections obtained from four WT mice or three *Pon3* KO mice.

significantly higher in Pon3 KD cells (Fig. 2*F*), suggesting enhanced channel proteolytic processing. Together, our data suggest that Pon3 regulates endogenous ENaC functional expression in mCCD cells.

### *Pon3 interacts with ENaC subunits*

We then performed coimmunoprecipitation to investigate whether PON3 forms a complex with ENaC subunits. Briefly, we transfected FRT cells with mouse Pon3 that had a C-termi-

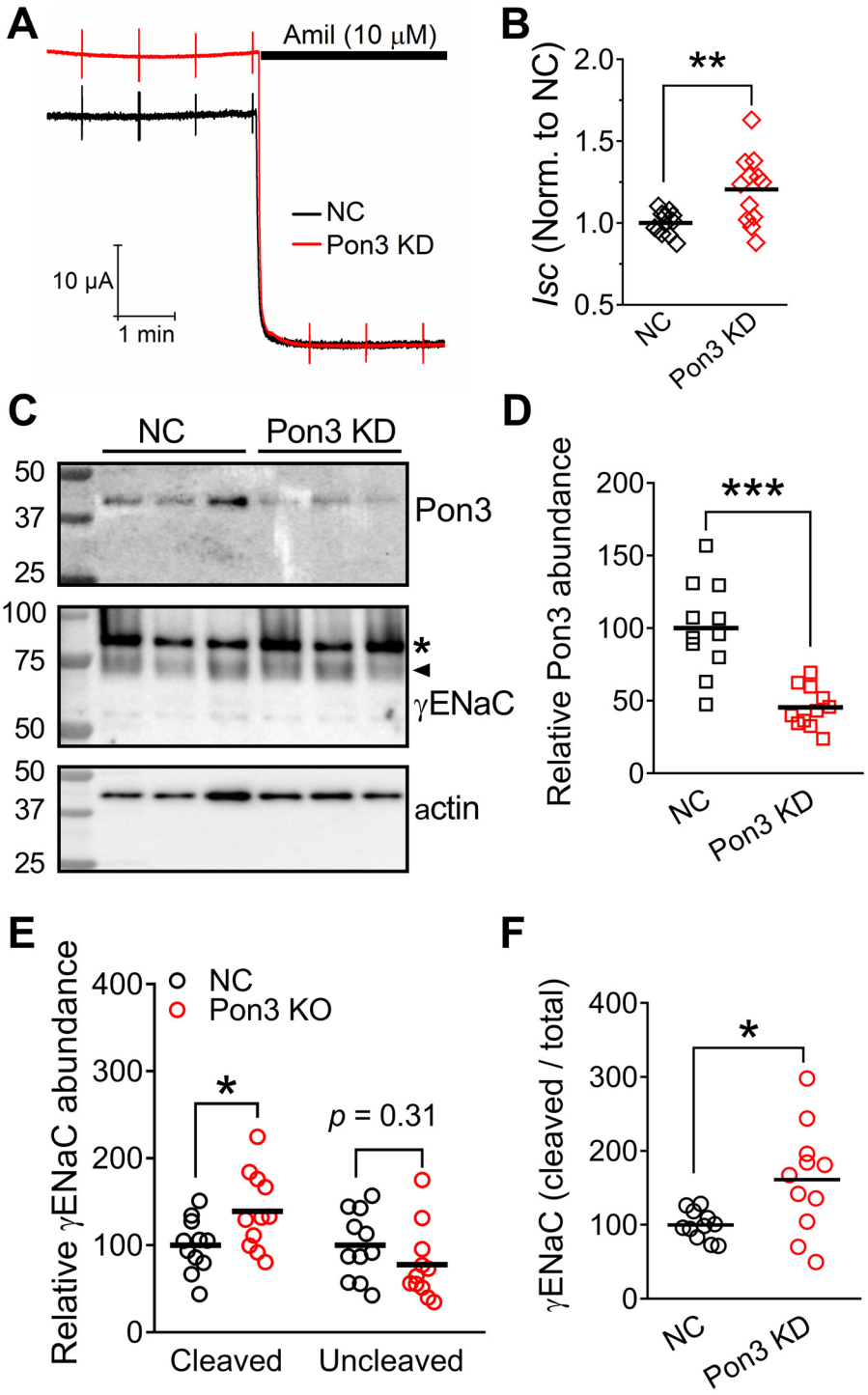


**Figure 2. Pon3 KD in mCCD cells enhances the functional expression of endogenous ENaC.** mCCD cells were transfected with *Pon3*-specific siRNA (*Pon3 KD*) or scrambled siRNA as an NC. Transfected cells were then cultured on permeable filters, and amiloride (*Amil*)-sensitive $I_{sc}$ were determined with an Ussing chamber assay. *A*, representative traces in NC cells (*black*) or Pon3 KD cells (*red*). After reaching a steady current, 10 μM amiloride (*black bar*) was added to the apical side of the Ussing chamber to block ENaC. *B*, summary of the amiloride-sensitive $I_{sc}$ of Pon3 KD cells normalized (*Norm.*) to the average $I_{sc}$ of NC cells from the same experiment. *C*, following the recordings, whole-cell lysates were collected from the filters to blot for γENaC, Pon3, and actin as a loading control. The *asterisk* and *arrowhead* indicate uncleaved and cleaved γENaC, respectively. *D* and *E*, whole-cell expression of Pon3 (*D*) and γENaC (*E*) were normalized to actin and are shown as a percentage of NC cells. *F*, to access the extent of γENaC cleavage, the ratio of the cleaved γENaC to total γENaC (cleaved and uncleaved) was estimated for each sample and is shown as a percentage of NC cells. Experiments were repeated a total of four times with three individual transfections of scrambled siRNA or Pon3 siRNA for each experiment. Data are shown in scatter-dot plots, with a *horizontal bar* indicating the mean. Statistical comparisons were analyzed with a nonparametric Mann–Whitney test or with one-way ANOVA followed by Sidak's multiple comparisons test. *, $p < 0.05$; **, $p < 0.01$; ***, $p < 0.001$.

nal Myc-FLAG epitope tag, mouse ENaC, or both. In each case, only one ENaC subunit had an N-terminal HA and a C-terminal V5 epitope tag ($_{HA}\alpha_{V5}\beta\gamma$, $\alpha_{HA}\beta_{V5}\gamma$, or $\alpha\beta_{HA}\gamma_{V5}$). Whole-cell lysates were either precipitated with anti-V5 antibodies to pull-down ENaC and probe for Pon3 (Fig. 3*A*) or precipitated with anti-FLAG antibodies to pulldown Pon3 and probe for ENaC

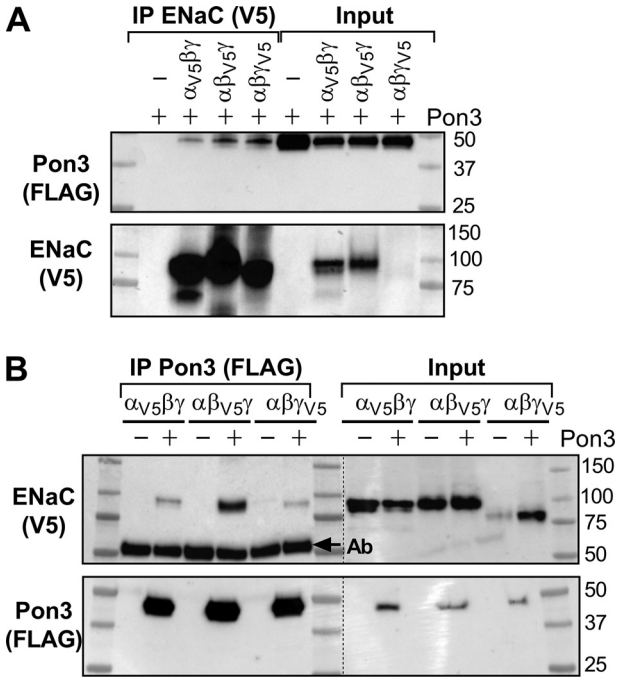


**Figure 3. Pon3 interacts with ENaC subunits in FRT cells.** FRT cells were transiently transfected with cDNAs encoding mouse Pon3 and/or ENaC subunits. In each case, only one ENaC subunit had a C-terminal V5, tag as indicated above. *Pon3* was cloned in the pCMV6 vector, which includes a C-terminal Myc-FLAG tag. *A*, whole-cell lysates were immunoprecipitated (*IP*) with anti-V5 antibodies to pull down ENaC and blotted for Pon3. *B*, vice versa, the lysates were immunoprecipitated with anti-FLAG antibodies to pull down Pon3 and blotted for ENaC subunits with V5 antibodies. The anti-FLAG antibody and the V5 antibody were raised in mice. The *arrow* indicates the heavy chain of the anti-FLAG antibody recognized by the secondary antibody. Expression of ENaC and Pon3 was also assessed in whole-cell lysates (*input*). *Vertical dashed lines* indicate that the same blot of different exposures is shown for immunoprecipitate and input. The mobility of the molecular mass standards (kilodaltons) is shown. Experiments were repeated three to for times for each condition.

subunits (Fig. 3*B*). As shown in Fig. 3*A*, Pon3-Myc-FLAG (~45 kDa) was detected in V5 precipitates of FRT cells coexpressing Pon3 and ENaC but not in cells transfected with only Pon3. Vice versa, ENaC subunits could be detected only in FLAG precipitates of FRT cells coexpressing Pon3 and ENaC but not in cells transfected with ENaC alone (Fig. 3*B*). Expression of Pon3 or ENaC subunits was detected in whole-cell lysate as expected (input). Our data suggest that Pon3 specifically interacts with ENaC subunits when coexpressed in FRT cells.

### *Pon3 reduces ENaC expression in FRT cells*

As ENaC functional expression was enhanced by Pon3 KD in mCCD cells, we examined whether overexpressing Pon3 affects ENaC expression in FRT cells. We cotransfected FRT cells with ENaC ($_{HA}\alpha_{V5}\beta\gamma$) with either the *Pon3* plasmid or an equal amount of the empty vector. Surface proteins were biotinylated on ice and recovered with NeutrAvidin beads. The expression of ENaC $\alpha$ and $\gamma$ subunits was assessed in surface precipitates and whole-cell lysates. GAPDH was absent in surface precipitates, indicating that the surface fractions were free of contamination from intracellular proteins (Fig. 4*A*, *bottom*). In FRT cells coexpressing Pon3, whole-cell ENaC expression was significantly lower for full-length $\alpha$ENaC (48% ± 22%, $n = 5–6$, $p < 0.01$), the cleaved $\alpha$ENaC (64% ± 14%, $n = 5–6$, $p < 0.001$) and $\gamma$ENaC (41% ± 13%, $n = 5–6$, $p < 0.01$, Fig. 4*B*). In contrast, Pon3 did not alter the ratio of surface abundance *versus* whole-cell abundance for $\alpha$ENaC or $\gamma$ENaC (Fig. 4*C*), suggesting that Pon3 not only reduced ENaC subunit whole-cell expression but also decreased channel density at the cell surface in FRT cells. This inhibitory effect of Pon3 is consistent with our findings of the effects of endogenous Pon3 on ENaC in mCCD cells (Fig. 2). As a control, we tested whether $\gamma$-glutamyl transferase ($\gamma$GT), an unrelated type II protein affects ENaC expression in FRT cells. Our data suggest that coexpressing mouse $\gamma$GT has no effect on ENaC abundance at the whole-cell level in FRT cells (Fig. 4, *D* and *E*).

### *Pon3 inhibits ENaC activity by reducing channel surface expression in Xenopus oocytes*

To further investigate the role of Pon3 in regulating ENaC functional expression, we injected mature oocytes with cRNA mixtures encoding WT ENaC alone or with an equal amount of mouse *Pon3* cRNA. Whole-cell $Na^+$ currents were measured 24–30 h after injection by clamping oocytes at −100 mV (Fig. 5*A*). The average amiloride-sensitive $Na^+$ current in oocytes coexpressing ENaC and Pon3 (−1.4 ± 1.4 $\mu$A, $n = 60$) is ~40% lower than in oocytes expressing ENaC alone (−2.4 ± 1.8 $\mu$A, $n = 62$, $p < 0.01$). This is similar to the extent of inhibition of PON2 on ENaC activity (57). The inhibitory effect of Pon3 is specific to ENaC, as Pon3 did not alter renal outer medullary $K^+$ (Romk) channel activity (−2.5 ± 1.8 $\mu$A in oocytes expressing Romk *versus* −2.2 ± 1.9 $\mu$A in oocytes coexpressing Pon3 and Romk, Fig. 5*C*).

The inhibitory effect of Pon3 on ENaC activity suggests a reduction in channel open probability ($P_O$) and/or in the number of functional channels at the cell surface. As Pon3 reduced ENaC surface expression in FRT cells (Fig. 4), we examined the effect of Pon3 on channel surface expression in oocytes using a FLAG epitope–tagged ENaC $\beta$ subunit, as described previously (69). As shown in Fig. 6*A*, the surface expression of the nontagged channel was 0.2 ± 0.5 × $10^6$ (shown as relative light units, $n = 21$) but rose to 1.6 ± 1.8 × $10^7$ in oocytes expressing FLAG-tagged ENaC ($n = 33$, $p < 0.0001$). Notably, this value was significantly reduced in oocytes coexpressing Pon3 (3.3 ± 3.3 × $10^6$, $n = 36$, $p < 0.01$). In contrast, whole-cell expression of $\beta$ENaC in oocytes was not altered by Pon3 (Fig. 6*C*).

### *Pon3 does not alter ENaC $P_O$ in Xenopus oocytes*

ENaC is gated in response to external cues, such as proteolytic cleavage, extracellular $Na^+$, and laminar shear stress, that primarily modulate channel $P_O$ (70, 71). Specific proteases activate ENaC by releasing the embedded inhibitory tracts from the $\alpha$ or $\gamma$ subunit, increasing channel $P_O$ (72–76). We examined whether Pon3 affects channel activation by a protease, $\alpha$-chymotrypsin. Oocytes were treated with $\alpha$-chymotrypsin (2 $\mu$g/ml) for 2 min until currents reached a steady state (Fig. 7*A*). If Pon3 reduces channel $P_O$, we predicted that the fold increase in ENaC current following $\alpha$-chymotrypsin treatment would be altered. However, we found that chymotrypsin elicited a 1.9 ± 1.0-fold increase in whole-cell $Na^+$ currents in oocytes expressing ENaC and a similar 1.9 ± 0.5-fold

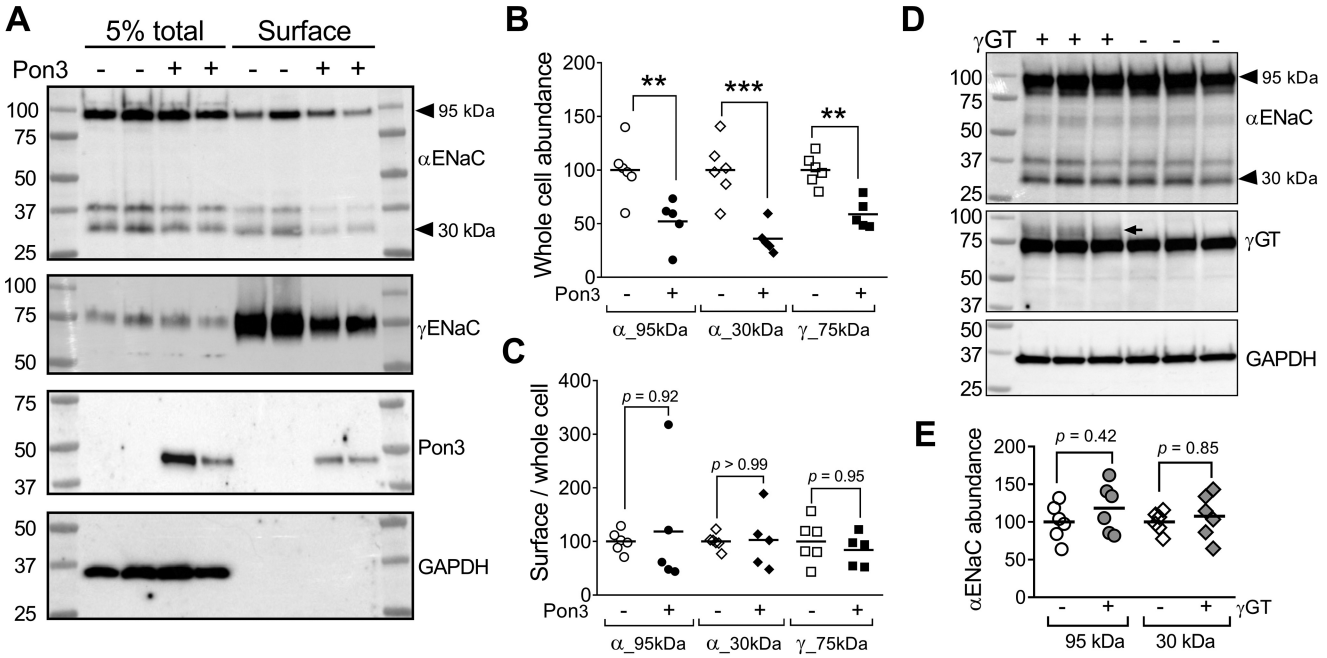


**Figure 4. Pon3 reduces ENaC surface and whole-cell expression in FRT cells.** *A*, FRT cells were transiently transfected with three ENaC subunits, where only the α subunit had an N-terminal HA tag and a C-terminal V5 tag. Equal amounts of the mouse *Pon3* plasmid or the pCMV6 vector were cotransfected. Surface ENaC was labeled with biotin and recovered with NeutrAvidin beads at 4 °C. Blots were probed for the α subunit, γ subunit, Pon3, or GAPDH in the biotinylated surface fraction and in 5% of the total whole-cell lysates. *B*, the abundance of the α subunit (full-length 95 kDa and cleaved 30 kDa, indicated by *arrowheads*) or the γ subunit (~75 kDa) in whole-cell lysate was normalized to the loading control (GAPDH) and expressed as the percentage in cells transfected with ENaC alone (−*Pon3*). *C*, the abundance of the α subunit (full-length 95 kDa and cleaved 30 kDa) or the γ subunit (~75 kDa) at the cell surface was normalized to whole-cell abundance of the α or γ subunit, respectively, and then expressed as the percentage in cells transfected with ENaC alone (−*Pon3*). *D*, as a control, FRT cells were cotransfected with $_{HA}\alpha_{V5}\beta\gamma$ and with either γ-glutamyl transferase (+*γGT*) or an equal amount of the pCDNA3 vector (−*γGT*). Whole-cell lysates were collected and probed for both αENaC and γGT (indicated by the *arrow*). *E*, the abundance of the α subunit (95 kDa and 30 kDa) was normalized to the loading control (GAPDH) and expressed as the percentage in cells transfected with ENaC alone (−*γGT*). Experiments were repeated a total of three times with FRT cells of different passages. The summarized data are shown in a scatter-dot plot, with a *horizontal bar* indicating the mean. Statistical comparisons were analyzed with one-way ANOVA followed by Sidak's multiple comparisons test (**, $p < 0.01$; ***, $p < 0.001$).

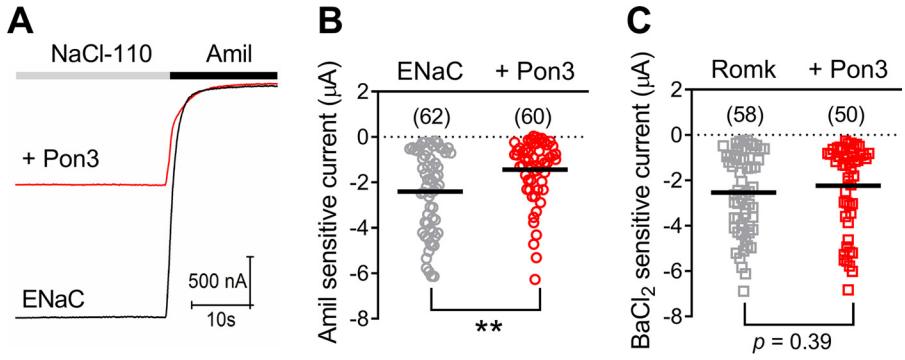


**Figure 5. Pon3 inhibits ENaC activity in oocytes.** A, representative traces of whole-cell $Na^+$ currents measured in oocytes expressing mouse ENaC alone (*black*) or coexpressing Pon3 (+Pon3, *red*), with the holding potential set at −100 mV. After reaching a steady current, 10 μM amiloride (*Amil*, *black bar*) was added to the bath to block ENaC. *B*, summary of the amiloride-sensitive $Na^+$ currents in oocytes expressing ENaC or ENaC and Pon3. *C*, summary of the $BaCl_2$-sensitive $K^+$ currents of oocytes injected with Romk with or without Pon3. Experiments were repeated with four batches of oocytes, and the pooled data are shown in scatter-dot plots, with a *horizontal bar* indicating the mean. The number of oocytes assessed for each condition is listed. Statistical comparisons were analyzed with nonparametric Mann–Whitney tests (**, $p < 0.01$).

increase in oocytes coexpressing ENaC and Pon3 (Fig. 7*C*). As a result, the post-α-chymotrypsin treatment currents were still lower in the presence of Pon3 (−2.7 ± 1.5 μA, $n$ = 21, $p < 0.0001$) compared with oocytes only expressing ENaC (−5.5 ± 2.3 μA, $n$ = 21).

To examine the effect of Pon3 on channel $P_O$ in a more direct manner, we measured the response of ENaC bearing a Cys mutation at the degenerin site of the β subunit ($\alpha\beta_{S518C}\gamma$) to [2-(trimethylammonium)ethyl]methanethiosulfonate MTSET. The activity of this channel rises when a disulfide bond is formed between MTSET and the introduced Cys within the channel pore, reflecting an increase in channel $P_O$ (77, 78). As shown in Fig. 8, the whole-cell $Na^+$ currents in oocytes expressing $\alpha\beta_{S518C}\gamma$ was increased 2.1 ± 0.7-fold by MTSET ($n$ = 16). The presence of Pon3 did not alter the effect of MTSET on ENaC activity, as a 2.0 ± 0.4-fold increase in whole-cell $Na^+$ currents was observed in oocytes coexpressing $\alpha\beta_{S518C}\gamma$ and Pon3 ($n$ = 16, Fig. 8*B*). Together, our data suggest that Pon3 inhibits ENaC activity in oocytes by reducing channel surface expression and not $P_O$.

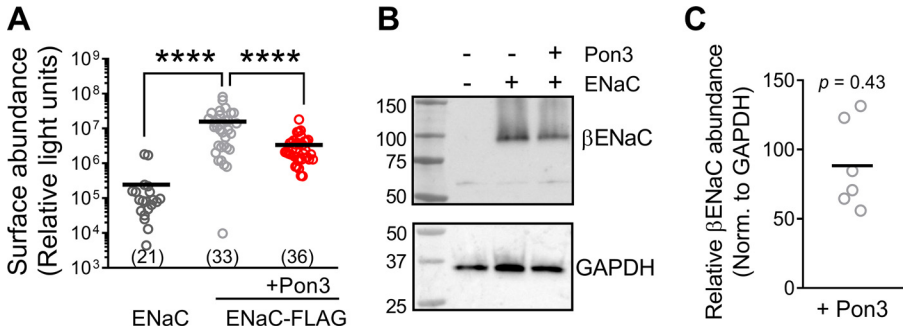


**Figure 6. Pon3 reduces ENaC surface expression in oocytes.** *A*, a chemiluminescence assay was performed to assess the surface abundance of ENaC in oocytes expressing WT (nontagged) ENaC, ENaC with a $\beta$ subunit bearing an extracellular FLAG tag (*ENaC*-FLAG), or ENaC-FLAG coexpressed with mouse Pon3. Relative light units measured for individual oocytes are shown. Experiments were repeated with oocytes harvested from three individual frogs. The number of oocytes assessed for each group is listed. Data are shown in a scatter-dot plot, with *horizontal bars* indicating the means. Statistical comparisons were analyzed with nonparametric Kruskal–Wallis test followed by Dunn's multiple comparisons test (**, $p < 0.01$; ****, $p < 0.0001$). *B*, $\beta$ENaC was probed in whole-cell homogenates of oocytes expressing ENaC or ENaC and Pon3 with the StressMarq $\beta$ antibody. Noninjected oocytes from the same batch were used as a negative control, and GAPDH was probed as a loading control. *C*, the expression of $\beta$ENaC in the presence or absence of Pon3 was normalized to GAPDH and then expressed as the percentage in oocytes expressing ENaC only (−Pon3) for individual experiments. Data are shown in a scatter-dot plot, with a *horizontal bar* indicating the mean. Experiments were repeated with six different batches of oocytes. No statistically significant difference was observed when data were analyzed with a nonparametric Wilcoxon signed-rank test.

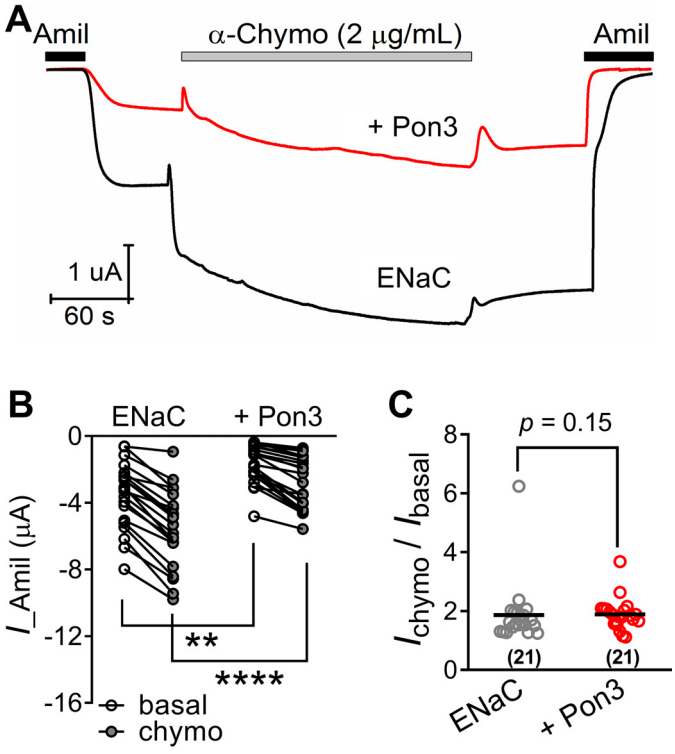


**Figure 7. Pon3 does not alter ENaC activation by $\alpha$-chymotrypsin.** *A*, superimposed traces from oocytes expressing mouse ENaC (*black*) or coexpressing mouse Pon3 (*red*). Oocytes were perfused with $\alpha$-chymotrypsin (*gray bar*, 2 $\mu$g/ml) for 2 min until the current reached a steady state. Amiloride (*Amil*) was added to the bath at the beginning and the end of each recording (*black bars*). *B*, amiloride-sensitive whole-cell $Na^+$ currents (*I_Amil*) measured prior to ($I_{basal}$) and following chymotrypsin treatment ($I_{chymo}$) are shown for individual oocytes. Statistical comparisons were analyzed with two-way ANOVA followed by Sidak's multiple comparisons test (**, $p < 0.01$; ****, $p < 0.0001$). *C*, the -fold increase of ENaC currents in response to $\alpha$-chymotrypsin ($I_{chymo}/I_{basal}$) was estimated for individual oocytes. Data pooled from three experiments are shown in a scatter-dot plot, with the *horizontal bar* indicating the mean. The number of oocytes assessed for each group is listed. Statistical comparisons were analyzed with a nonparametric Mann–Whitney test.

## Discussion

PON family members are encoded by highly conserved genes, although the three members have distinct substrate specificities and tissue expression (46, 47, 51). A recent study by Clark and co-workers (79) identified convergent functional loss of *PON1* but not *PON2* or *PON3* in marine mammals. *PON1* contained lesions within the coding region, rendering marine mammals susceptible to neurotoxicity induced by organophosphorus compounds. In contrast, *PON1* was intact in all 53 surveyed terrestrial mammal genomes (79). Like PON1, PON3 is highly expressed in the gallbladder and liver (80), and *Pon3* KO mice exhibit altered metabolism of lipid and bile acids. They are also susceptible to developing obesity, atherosclerosis, and large gallstones when fed a diet containing cholic acid and cholesterol (81). ENaC and the bile acid–sensitive ion channel, a related member of the ENaC/degenerin family, are expressed in cholangiocytes lining bile ducts, and their channel activities can be regulated by unconjugated and conjugated bile acids (82–85).

As the least-studied member in the PON family, little is known about the expression or function of PON3 in other organs, such as the kidneys. We show, for the first time, that Pon3 is specifically expressed in distal nephron segments of mouse kidneys, including the DCT2, CNT, and CD. These are the same nephron segments where ENaC resides. In the CNT and CD, fine-tuning of $Na^+$ reabsorption takes place under the control of aldosterone (86–93). Interestingly, we observed differential expression of Pon3 in distal nephron segments. It appears to have homogeneous expression within the NCC-positive DCT2 and $CaBP_{28K}$-positive CNT, where Pon3 is nearly present in all cells lining these tubules. In contrast, Pon3 has higher expression in V-ATPase-positive ICs than in AQP2-positive PCs of CDs. This is consistent with a previous study showing that higher levels of *Pon3* transcripts were found in ICs of mouse CDs (60). In addition, the expression of Pon3 is quite variable in PCs of CDs, with only ~25% cells coexpressing both Pon3 and AQP2.

This is particularly intriguing because the magnitude of ENaC-mediated $Na^+$ reabsorption differs in these segments. It has been shown that CD-specific $\alpha$ENaC KO mice were able to maintain normal $Na^+/K^+$ homeostasis when challenged with dietary salt/water restriction (94). When $\alpha$ENaC was deleted in the CNT and CD, KO mice developed a severe salt-wasting phenotype and a continuous reduction in body weight (95). In

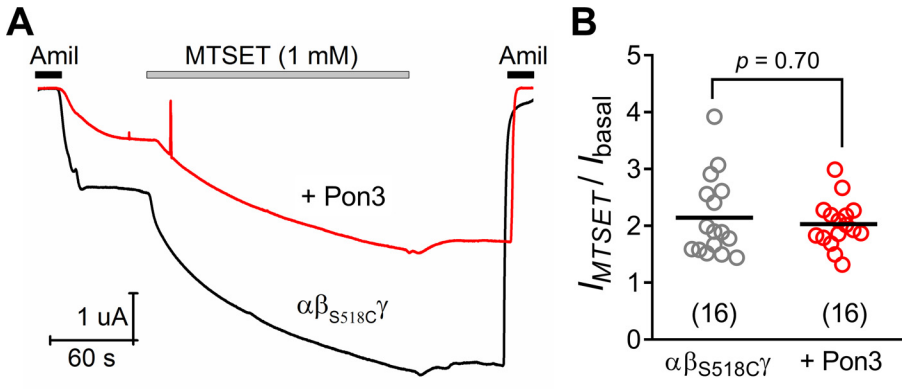


**Figure 8. Pon3 does not affect ENaC gating in response to MTSET modification.** *A*, recordings from oocytes expressing mouse $\alpha\beta_{S518C}\gamma$ alone (*black*) or coexpressing Pon3 (*red*) are superimposed. Freshly prepared MTSET (1 mM) was applied to oocytes via perfusion to modify the introduced -SH group at the degenerin site of the $\beta$ subunit (S518C, *gray bar*). At the beginning and end of each recording, 10 $\mu$M amiloride (*Amil*) was added to the bath to block ENaC activity (*black bars*). *B*, the -fold increase of ENaC currents elicited by MTSET ($I_{MTSET}/I_{basal}$) was estimated for individual oocytes harvested from three different frogs. Pooled data are shown in a scatter-dot plot, with the *horizontal bar* indicating the mean. The number of oocytes assessed for each group is listed. Statistical comparisons were analyzed with a nonparametric Mann–Whitney test.

addition, ENaC currents are significantly greater in the CNT compared with the cortical CD (96, 97). Together, these studies suggest that ENaC expression in the CNT has a key role in $Na^+$ homeostasis in mice. As PON3 is mainly expressed in principal cells of the CNT, we predict that PON3 has an important role in regulating renal $Na^+/K^+$ homeostasis and BP control.

This study examined the role of PON3 in regulating ENaC functional expression in different expression systems. We found that Pon3 KD in mCCD cells led to enhanced amiloride-sensitive $Na^+$ transport, a higher abundance of a cleaved γENaC product (~75 kDa), and higher ratios of cleaved γENaC *versus* total γENaC, suggesting up-regulation of ENaC proteolytic processing and surface expression in mCCD cells when Pon3 expression was reduced. Supporting this notion, surface expression of ENaC subunits was reduced by Pon3 coexpression in FRT cells and *Xenopus* oocytes. It is interesting to note that the anti-γENaC antibody recognized two forms (cleaved and uncleaved) of endogenous γENaC in mCCD cells but favored cleaved γENaC when ENaC was overexpressed in FRT cells. Nonetheless, our results using cultured epithelial cells or *Xenopus* oocytes support that PON3 decreases ENaC functional expression. Other members of this family, including PON2 and MEC-6, also inhibit ENaC activity in oocytes (57). This negative regulation of channel activity is of great interest to us, as ENaC hyperactivity has physiological consequences (11, 13, 98–101). There is growing evidence suggesting that members of the PON family, including MEC-6, PON2, and PON3, function as chaperones to modulate the expression of ion channels within the ENaC/degenerin family (56, 57). MEC-6 is not only required for proper folding and assembly of MEC-4 channels but also to facilitate channel surface expression (56). Little is known regarding the chaperone function of PONs. We found that coexpression of Pon3 reduced ENaC whole-cell expression in FRT cells, suggesting that this trimeric channel is less stable in the presence of Pon3. Molecular chaperones have important roles in ENaC quality control within the early secretory pathway (34, 42, 102). It is possible that PON3 facilitates proteasomal degradation of misfolded ENaC subunits. Other chaperones have been identified that affect ENaC trafficking at later sites in the secretory pathway (40, 41, 43, 44, 103). Additional studies are needed to investigate mechanisms by which PONs regulate ENaC expression and the physiological relevance of this regulation in the kidneys and other organs.

## Experimental procedures

### Plasmids

Mouse *Pon3* was cloned in the pCMV6 vector (MR220409, OriGene) and has a C-terminal Myc-FLAG tag. The mouse ENaC α, β, and γ subunits with an N-terminal HA epitope tag and a C-terminal V5 epitope tag were cloned in the pcDNA3 vector and used to transfect FRT cells. WT or mutant mouse ENaC α, β, and γ subunits cloned in the pBlueScript vector were used for expressing ENaC in oocytes. Mouse γGT was cloned in the pcDNA3 vector (104).

### Tissue immunofluorescence staining

Kidneys from WT C57BL/6 mice or *Pon3* KO mice (The Jackson Laboratory, 027311) were harvested using a protocol approved by the University of Pittsburgh Institutional Animal Care and Use Committee. Formalin-fixed kidney tissue was embedded in paraffin and cut into 4-μm-thick serial sections. After deparaffinization and rehydration, the tissues were blocked with 10% horse serum to block nonspecific staining. Kidney sections were incubated with the following primary antibodies overnight at 4 °C: goat anti-PON3 (2 μg/ml, R&D Systems, AF4345), rabbit anti-Na–K–Cl cotransporter (1 μg/ml, StressMarq, SPC401), guinea pig anti-parvalbumin (2 μg/ml, Swant, GP72), rabbit anti-NCC (2 μg/ml, StressMarq, SPC401), rabbit anti-$CaBP_{28K}$ (0.5 μg/ml, Proteintech, 144791AP), rabbit anti-AQP2 (0.6 μg/ml, Alomone Labs, AQP-002), and rabbit anti-V-ATPase E1 subunit (1 μg/ml, Invitrogen, PA5-29899). The sections were subsequently incubated with fluorescent secondary donkey antibodies (anti-guinea pig Alexa 647 (2 μg/ml), anti-goat Alexa 488 (4 μg/ml), or anti-rabbit Cy3 (2 μg/ml), Jackson ImmunoResearch Laboratories) for 2 h at room temperature. A Leica SP8 confocal microscope was used to image transverse sectioned kidneys from the cortex to the medulla using a tile scan technique and a 40× oil, 1.3 numerical aperture objective. Other images were acquired with a Leica DM6000B wide-field microscope with a

Retiga 4000R Fast 1394 camera. To quantify Pon3 expression in specific nephron segments and cell types, the staining was repeated with kidney tissues from four WT mice, and four or five fields were chosen randomly for each kidney sample. The fluorescence intensity of Pon3 staining in glomeruli was used as the threshold to identify positive Pon3 staining. Numbers of total cells as well as cells with positive staining of Pon3 and/or the chosen markers were manually counted for each individual PON3-positive tubule in the field. The specificity of the anti-PON3 antibody was examined in kidney sections from *Pon3* KO mice.

### mCCD cells, siRNA KD, and Ussing chamber recording

mCCD cells were grown in DMEM/F12 medium (Gibco, 21041) supplemented with insulin (5 $\mu$g/ml), human apotransferrin (5 $\mu$g/ml), epidermal growth factor (10 ng/ml), tri-iodothyronine (1 nM), dexamethasone (50 nM), sodium selenite (0.06 nM), and 2% decomplemented FBS at 37 °C in 5% $CO_2$ as described previously (105). For KD experiments, cells were reverse-transfected with 50 pmol of a control siRNA of scrambled sequence or a dicer-specific siRNA targeting the mouse *Pon3* sequence 5′-GUACUAUAUUUCACAAAGCUCUGTA-3′ (Integrated DNA Technologies) on permeable Snapwell filters (1.12-$cm^2$ surface area) using Lipofectamine 3000 (L3000008, Invitrogen) according to the manufacturer's instructions. Transfected cells were cultured for an additional 4 days to fully polarize before being mounted onto modified Ussing chambers (P2302, Physiological Instruments) for electrophysiology experiments.

The hemichambers contained 5 ml of Krebs buffer solution (110 mM NaCl, 25 mM $NaHCO_3$, 5.8 mM KCl, 2 mM $MgSO_4$, 1.2 mM $K_2HPO_4$, 2 mM $CaCl_2$, and 11 mM glucose) in both sides. The hemichambers were continuously bubbled with 95% $O_2$, 5% $CO_2$, which maintained the pH at 7.4 and the temperature at 37 °C. $I_{sc}$ was measured under voltage clamp conditions. After $I_{sc}$ reached a stable state, 10 $\mu$M amiloride was added to the apical side. To calculate the transepithelial resistance, a bipolar pulse of 10 mV with a duration of 0.5 s was applied every 60 s. All filters were recovered to collect whole-cell lysates with a detergent solution (20 mM HEPES, 100 mM NaCl, 40 mM KCl, 1 mM EDTA, 10% glycerol, 1% NP40, and 0.4% deoxycholate (pH 7.4)) supplemented with protease inhibitor mixture III (535140, Calbiochem). Whole-cell lysates were subjected to SDS-PAGE under reducing conditions to probe for the endogenous Pon3 (0.1 $\mu$g/ml, Sigma, HPA014848), γENaC (1 $\mu$g/ml, StressMarq, SPC-405), or actin (0.2 $\mu$g/ml, Sigma, A1978). Immunoblots were developed using Clarity Western ECL blotting substrate (1705060, Bio-Rad) and imaged with Bio-Rad ChemiDoc™.

### FRT cell coimmunoprecipitation and surface biotinylation

FRT cells were cultured in DMEM/F12 medium supplemented with 8% FBS. For the coimmunoprecipitation assay, FRT cells were seeded on 6-well dishes and transfected with plasmids encoding mouse Pon3 and mouse ENaC subunits (0.5 $\mu$g/construct). In each case, only one ENaC subunit had an N-terminal HA tag and a C-terminal V5 epitope tag ($_{HA}\alpha_{V5}\beta\gamma$, $\alpha_{HA}\beta_{V5}\gamma$ or $\alpha\beta_{HA}\gamma_{V5}$). The next day, cells were extracted with detergent solution supplemented with protease inhibitor mixture. Five percent of the cell lysate was saved as input. The remainder was incubated overnight with 50 $\mu$l of agarose-immobilized anti-V5 antibodies (S190-119, Bethyl) with end-over-end mixing at 4 °C to pull down ENaC subunits. To pull down Pon3, the lysates were incubated with anti-FLAG antibodies (2 $\mu$g, F3165, Sigma) in the presence of rec-protein G–Sepharose (10-1241, Invitrogen). Proteins were eluted into Laemmli sample buffer (1610737, Bio-Rad) by heating the isolated beads at 95 °C. The immunoprecipitate and the input were subjected to SDS-PAGE and blotted for Pon3 (0.1 $\mu$g/ml, Sigma, HPA014848) or for ENaC subunits with V5 antibody (0.2 $\mu$g/ml, Invitrogen, R96025). Assays were repeated three times for each condition.

To measure surface expression of ENaC, FRT cells were transfected with plasmids encoding mouse $_{HA}\alpha_{V5}\beta\gamma$ with or without the *Pon3* plasmid (0.5 $\mu$g/construct) directly on 24-mm Transwell filters and cultured to confluency. In the control group, an equal amount of the pCMV6 vector was included. FRT cells grown on the filters were washed four times with cold Dulbecco's PBS with 1.0 mM $CaCl_2$ and 0.5 mM $MgCl_2$ (PBS, Corning Life Sciences). To label apical surface proteins, 1 mg/ml EZ-Link™ Sulfo-NHS-SS-Biotin (21331, Thermo Fisher) in a buffer containing 137 mM NaCl and 15 mM sodium borate (pH 9.0) was added to the apical side, whereas the basolateral side was incubated with just the buffer. Excess biotin was then quenched with 10% FBS in DMEM/F12. After washing with PBS, cells were lysed in detergent solution and incubated with NeutrAvidin agarose (29200, Thermo Fisher) overnight at 4 °C to isolate biotinylated proteins. The recovered surface proteins and 5% of the total lysate were separated by SDS-PAGE and blotted for the α subunit with HA-HRP antibodies (0.05 $\mu$g/ml, 3F10, Sigma), the γ subunit (0.3 $\mu$g/ml, StressMarq), PON3 (0.03 $\mu$g/ml, Sigma), or GAPDH (0.3 $\mu$g/ml, Proteintech, HRP-60004), as described previously (29, 106).

In some experiments, FRT cells seeded on 6-well size plates were transfected with plasmids encoding mouse ENaC ($_{HA}\alpha_{V5}\beta\gamma$) or mouse γGT (0.5 $\mu$g/construct). An equal amount of the pCDNA3 vector was used in the control (−γGT) group. The next day, whole-cell lysates were extracted with detergent solution supplemented with protease inhibitors and subjected to SDS-PAGE. αENaC was detected with HA-HRP antibodies (0.05 $\mu$g/ml, 3F10, Sigma). γGT was detected using a rabbit polyclonal antibody described previously (107).

### Xenopus oocyte expression, two-electrode voltage clamp, and surface expression

cRNAs of mouse ENaC α, β, and γ subunits; mouse Pon3; and rat Romk were synthesized using mMESSAGE mMACHINE™ transcription kits (Invitrogen) following the manufacturer's protocol. Oocytes were harvested from *Xenopus laevis* following a protocol approved by the University of Pittsburgh Institutional Animal Care and Use Committee. Stage V-VI oocytes were injected with 2 ng of cRNA per ENaC subunit or 1 ng of rat Romk cRNA. An equal amount of mouse Pon3 cRNA was injected for the coexpression assay. The injected oocytes were incubated in modified Barth's saline (88 mM NaCl, 1 mM KCl, 2.4 mM $NaHCO_3$, 15 mM HEPES, 0.3 mM $Ca(NO_3)_2$, 0.41 mM $CaCl_2$, 0.82 mM $MgSO_4$, 10 $\mu$g/ml sodium penicillin, 10 $\mu$g/ml streptomycin sulfate, and 100 $\mu$g/ml gen-

tamycin sulfate (pH 7.4)) at 18 °C for an additional 24–48 h for optimal channel expression. Whole-cell $Na^+$ currents were measured by clamping oocytes at −100 mV, whereas oocytes were continuously perfused with a solution containing 110 mM NaCl, 2 mM KCl, 1.6 mM $CaCl_2$, and 10 mM HEPES (pH adjusted to 7.4). To examine the effect of Pon3 on ENaC gating in response to MTSET, oocytes were injected with cRNAs encoding the WT mouse ENaC $\alpha$ and $\gamma$ subunits and the degenerin mutation $\beta_{S518C}$ with or without an equal amount of mouse Pon3 cRNA. MTSET was freshly prepared and delivered to oocytes through perfusion. To measure the Pon3 effect on Romk activity, we replaced the NaCl in the perfusion solution with 100 mM KCl. At the end of each recording, $BaCl_2$ was applied at a final concentration of 5 mM to block Romk activity. Voltage clamping was performed using a GeneClamp 500B amplifier and Digi-Data 1440A interface (Molecular Devices). Electrophysiological data were analyzed with Clampfit 10.5 and plotted with Origin 2015 (OriginLab).

ENaC surface expression in oocytes was measured using a chemiluminescence assay as described previously (69). The mouse ENaC $\beta$ subunit with an extracellular FLAG epitope tag was included in the cRNA mixture. A nontagged WT $\beta$ subunit was used as a negative control. Surface expression was assessed 2 days after cRNA injection by incubating oocytes with anti-FLAG M2 antibodies (1 $\mu$g/ml, Sigma F3165) and then with anti-mouse HRP antibodies (1 $\mu$g/ml, Jackson ImmunoResearch Laboratories, 115036072). Chemiluminescence of each oocyte was developed with Super Signal ELISA Femto Maximum Sensitivity Substrate (37075, Thermo Scientific) and quantified as relative light units with a GloMax-Multi detection system (Promega). To investigate the effect of Pon3 on ENaC whole-cell expression, oocytes injected with ENaC or ENaC and Pon3 were homogenized, and whole-cell lysates were subjected to SDS-PAGE to probe for $\beta$ENaC (1 $\mu$g/ml, StressMarq, SPC-404D) or GAPDH (0.3 $\mu$g/ml). All oocytes experiments were repeated at least three times using different frogs.

### Statistical analyses

Data were expressed as the mean ± S.D. in the main text and are shown as scatter-dot plots, with a horizontal bar indicating the mean. Data distribution was examined with a D'Agostino–Pearson normality test. Statistical comparisons between two groups were determined with a nonparametric Mann–Whitney test. Statistical comparisons between three or more groups were performed with one-way or two-way ANOVA, followed by Dunn's or Sidak's multiple comparisons test, using Prism 8 (GraphPad Software, San Diego, CA). $p < 0.05$ was considered statistically significant

*Author contributions*—S. S. and T. R. K. conceptualization; S. S., N. M., X. W., B. M. R., A. L. M., and C. J. B. data curation; S. S., N. M., and X. W. formal analysis; S. S. and T. R. K. supervision; S. S., C. J. B., and T. R. K. funding acquisition; S. S. validation; S. S. investigation; S. S., C. J. B., and R. J. T. visualization; S. S. writing-original draft; S. S. and T. R. K. project administration; S. S., N. M., C. J. B., R. J. T., M. D. C., and T. R. K. writing-review and editing; B. M. R., A. L. M., C. J. B., R. J. T., and M. D. C. methodology; M. D. C. resources.

*Acknowledgments—The γGT plasmid and the rabbit anti-γGT antibody were generous gifts from Dr. Rebecca P. Hughey from the Renal-Electrolyte Division at the University of Pittsburgh. We thank Dr. Hughey and Carol L. Kinlough for technical assistance with biochemical studies.*

### References

1. Duc, C., Farman, N., Canessa, C. M., Bonvalet, J. P., and Rossier, B. C. (1994) Cell-specific expression of epithelial sodium channel α, β, and γ subunits in aldosterone-responsive epithelia from the rat: localization by *in situ* hybridization and immunocytochemistry. *J. Cell Biol.* **127,** 1907–1921
2. McDonald, F. J., Snyder, P. M., McCray, P. B., Jr., and Welsh, M. J. (1994) Cloning, expression, and tissue distribution of a human amiloride-sensitive $Na^+$ channel. *Am. J. Physiol.* **266,** L728–L734 Medline
3. McDonald, F. J., Price, M. P., Snyder, P. M., and Welsh, M. J. (1995) Cloning and expression of the β- and γ-subunits of the human epithelial sodium channel. *Am. J. Physiol.* **268,** C1157–C1163 CrossRef Medline
4. Schild, L. (2010) The epithelial sodium channel and the control of sodium balance. *Biochim. Biophys. Acta* **1802,** 1159–1165 CrossRef Medline
5. Schild, L. (1996) The ENaC channel as the primary determinant of two human diseases: Liddle syndrome and pseudohypoaldosteronism. *Nephrologie* **17,** 395–400 Medline
6. Hummler, E. (1999) Implication of ENaC in salt-sensitive hypertension. *J Steroid Biochem. Mol. Biol.* **69,** 385–390 CrossRef Medline
7. Su, Y. R., and Menon, A. G. (2001) Epithelial sodium channels and hypertension. *Drug Metab. Dispos.* **29,** 553–556 Medline
8. Bhalla, V., and Hallows, K. R. (2008) Mechanisms of ENaC regulation and clinical implications. *J. Am. Soc. Nephrol.* **19,** 1845–1854 CrossRef Medline
9. Hummler, E., Barker, P., Gatzy, J., Beermann, F., Verdumo, C., Schmidt, A., Boucher, R., and Rossier, B. C. (1996) Early death due to defective neonatal lung liquid clearance in α-ENaC-deficient mice. *Nat. Genet.* **12,** 325–328 CrossRef Medline
10. Donaldson, S. H., Hirsh, A., Li, D. C., Holloway, G., Chao, J., Boucher, R. C., and Gabriel, S. E. (2002) Regulation of the epithelial sodium channel by serine proteases in human airways. *J. Biol. Chem.* **277,** 8338–8345 CrossRef Medline
11. Myerburg, M. M., Butterworth, M. B., McKenna, E. E., Peters, K. W., Frizzell, R. A., Kleyman, T. R., and Pilewski, J. M. (2006) Airway surface liquid volume regulates ENaC by altering the serine protease-protease inhibitor balance: a mechanism for sodium hyperabsorption in cystic fibrosis. *J. Biol. Chem.* **281,** 27942–27949 CrossRef Medline
12. Donaldson, S. H., and Boucher, R. C. (2007) Sodium channels and cystic fibrosis. *Chest* **132,** 1631–1636 CrossRef Medline
13. Shimkets, R. A., Warnock, D. G., Bositis, C. M., Nelson-Williams, C., Hansson, J. H., Schambelan, M., Gill, J. R., Jr., Ulick, S., Milora, R. V., and Findling, J. W. (1994) Liddle's syndrome: heritable human hypertension caused by mutations in the β subunit of the epithelial sodium channel. *Cell* **79,** 407–414 CrossRef Medline
14. Hansson, J. H., Schild, L., Lu, Y., Wilson, T. A., Gautschi, I., Shimkets, R., Nelson-Williams, C., Rossier, B. C., and Lifton, R. P. (1995) A *de novo* missense mutation of the β subunit of the epithelial sodium channel causes hypertension and Liddle syndrome, identifying a proline-rich segment critical for regulation of channel activity. *Proc. Natl. Acad. Sci. U.S.A.* **92,** 11495–11499 CrossRef Medline
15. Lifton, R. P. (1995) Genetic determinants of human hypertension. *Proc. Natl. Acad. Sci. U.S.A.* **92,** 8545–8551 CrossRef Medline
16. Hansson, J. H., Nelson-Williams, C., Suzuki, H., Schild, L., Shimkets, R., Lu, Y., Canessa, C., Iwasaki, T., Rossier, B., and Lifton, R. P. (1995) Hypertension caused by a truncated epithelial sodium channel γ subunit: genetic heterogeneity of Liddle syndrome. *Nat. Genet.* **11,** 76–82 CrossRef Medline

17. Corvol, P. (1995) Liddle's syndrome: heritable human hypertension caused by mutations in the β subunit of the epithelial sodium channel. *J. Endocrinol. Invest.* **18,** 592–594 CrossRef Medline
18. Strautnieks, S. S., Thompson, R. J., Gardiner, R. M., and Chung, E. (1996) A novel splice-site mutation in the γ subunit of the epithelial sodium channel gene in three pseudohypoaldosteronism type 1 families. *Nat. Genet.* **13,** 248–250 CrossRef Medline
19. Chang, S. S., Grunder, S., Hanukoglu, A., Rösler, A., Mathew, P. M., Hanukoglu, I., Schild, L., Lu, Y., Shimkets, R. A., Nelson-Williams, C., Rossier, B. C., and Lifton, R. P. (1996) Mutations in subunits of the epithelial sodium channel cause salt wasting with hyperkalaemic acidosis, pseudohypoaldosteronism type 1. *Nat. Genet.* **12,** 248–253 CrossRef Medline
20. Strautnieks, S. S., Thompson, R. J., Hanukoglu, A., Dillon, M. J., Hanukoglu, I., Kuhnle, U., Seckl, J., Gardiner, R. M., and Chung, E. (1996) Localisation of pseudohypoaldosteronism genes to chromosome 16p12.2–13.11 and 12p13.1-pter by homozygosity mapping. *Hum. Mol. Genet.* **5,** 293–299 CrossRef Medline
21. Boscardin, E., Perrier, R., Sergi, C., Maillard, M. P., Loffing, J., Loffing-Cueni, D., Koesters, R., Rossier, B. C., and Hummler, E. (2018) Plasma potassium determines NCC abundance in adult kidney-specific γENaC knockout. *J. Am. Soc. Nephrol.* **29,** 977–990 Medline
22. Grimm, P. R., Coleman, R., Delpire, E., and Welling, P. A. (2017) Constitutively active SPAK causes hyperkalemia by activating NCC and remodeling distal tubules. *J. Am. Soc. Nephrol.* **28,** 2597–2606 CrossRef Medline
23. Rengarajan, S., Lee, D. H., Oh, Y. T., Delpire, E., Youn, J. H., and McDonough, A. A. (2014) Increasing plasma [$K^+$] by intravenous potassium infusion reduces NCC phosphorylation and drives kaliuresis and natriuresis. *Am. J. Physiol. Renal Physiol.* **306,** F1059–F1068 CrossRef Medline
24. Hadchouel, J., Soukaseum, C., Büsst, C., Zhou, X. O., Baudrie, V., Zürrer, T., Cambillau, M., Elghozi, J. L., Lifton, R. P., Loffing, J., and Jeunemaitre, X. (2010) Decreased ENaC expression compensates the increased NCC activity following inactivation of the kidney-specific isoform of WNK1 and prevents hypertension. *Proc. Natl. Acad. Sci. U.S.A.* **107,** 18109–18114 CrossRef Medline
25. Canessa, C. M., Schild, L., Buell, G., Thorens, B., Gautschi, I., Horisberger, J. D., and Rossier, B. C. (1994) Amiloride-sensitive epithelial $Na^+$ channel is made of three homologous subunits. *Nature* **367,** 463–467 CrossRef Medline
26. Noreng, S., Bharadwaj, A., Posert, R., Yoshioka, C., and Baconguis, I. (2018) Structure of the human epithelial sodium channel by cryo-electron microscopy. *Elife* CrossRef
27. Waldmann, R., Champigny, G., Bassilana, F., Voilley, N., and Lazdunski, M. (1995) Molecular cloning and functional expression of a novel amiloride-sensitive $Na^+$ channel. *J. Biol. Chem.* **270,** 27411–27414 CrossRef Medline
28. Giraldez, T., Afonso-Oramas, D., Cruz-Muros, I., Garcia-Marin, V., Pagel, P., González-Hernández, T., and Alvarez de la Rosa, D. (2007) Cloning and functional expression of a new epithelial sodium channel δ subunit isoform differentially expressed in neurons of the human and monkey telencephalon. *J. Neurochem.* **102,** 1304–1315 CrossRef Medline
29. Heidrich, E., Carattino, M. D., Hughey, R. P., Pilewski, J. M., Kleyman, T. R., and Myerburg, M. M. (2015) Intracellular $Na^+$ regulates epithelial $Na^+$ channel maturation. *J. Biol. Chem.* **290,** 11569–11577 CrossRef Medline
30. Mueller, G. M., Kashlan, O. B., Bruns, J. B., Maarouf, A. B., Aridor, M., Kleyman, T. R., and Hughey, R. P. (2007) Epithelial sodium channel exit from the endoplasmic reticulum is regulated by a signal within the carboxyl cytoplasmic domain of the α subunit. *J. Biol. Chem.* **282,** 33475–33483 CrossRef Medline
31. Hughey, R. P., Bruns, J. B., Kinlough, C. L., and Kleyman, T. R. (2004) Distinct pools of epithelial sodium channels are expressed at the plasma membrane. *J. Biol. Chem.* **279,** 48491–48494 CrossRef Medline
32. Hughey, R. P., Mueller, G. M., Bruns, J. B., Kinlough, C. L., Poland, P. A., Harkleroad, K. L., Carattino, M. D., and Kleyman, T. R. (2003) Maturation of the epithelial $Na^+$ channel involves proteolytic processing of the α- and γ-subunits. *J. Biol. Chem.* **278,** 37073–37082 CrossRef Medline
33. Valentijn, J. A., Fyfe, G. K., and Canessa, C. M. (1998) Biosynthesis and processing of epithelial sodium channels in *Xenopus* oocytes. *J. Biol. Chem.* **273,** 30344–30351 CrossRef Medline
34. Buck, T. M., Kolb, A. R., Boyd, C. R., Kleyman, T. R., and Brodsky, J. L. (2010) The endoplasmic reticulum-associated degradation of the epithelial sodium channel requires a unique complement of molecular chaperones. *Mol. Biol. Cell* **21,** 1047–1058 CrossRef Medline
35. Buck, T. M., Jordahl, A. S., Yates, M. E., Preston, G. M., Cook, E., Kleyman, T. R., and Brodsky, J. L. (2017) Interactions between intersubunit transmembrane domains regulate the chaperone-dependent degradation of an oligomeric membrane protein. *Biochem. J.* **474,** 357–376 CrossRef Medline
36. Malik, B., Schlanger, L., Al-Khalili, O., Bao, H. F., Yue, G., Price, S. R., Mitch, W. E., and Eaton, D. C. (2001) Enac degradation in A6 cells by the ubiquitin-proteosome proteolytic pathway. *J. Biol. Chem.* **276,** 12903–12910 CrossRef Medline
37. Staub, O., Abriel, H., Plant, P., Ishikawa, T., Kanelis, V., Saleki, R., Horisberger, J. D., Schild, L., and Rotin, D. (2000) Regulation of the epithelial $Na^+$ channel by Nedd4 and ubiquitination. *Kidney Int.* **57,** 809–815 CrossRef Medline
38. Kabra, R., Knight, K. K., Zhou, R., and Snyder, P. M. (2008) Nedd4-2 induces endocytosis and degradation of proteolytically cleaved epithelial $Na^+$ channels. *J. Biol. Chem.* **283,** 6033–6039 CrossRef Medline
39. Rotin, D., Kanelis, V., and Schild, L. (2001) Trafficking and cell surface stability of ENaC. *Am. J. Physiol. Renal Physiol.* **281,** F391–F399 CrossRef Medline
40. Kashlan, O. B., Mueller, G. M., Qamar, M. Z., Poland, P. A., Ahner, A., Rubenstein, R. C., Hughey, R. P., Brodsky, J. L., and Kleyman, T. R. (2007) Small heat shock protein αA-crystallin regulates epithelial sodium channel expression. *J. Biol. Chem.* **282,** 28149–28156 CrossRef Medline
41. Chanoux, R. A., Robay, A., Shubin, C. B., Kebler, C., Suaud, L., and Rubenstein, R. C. (2012) Hsp70 promotes epithelial sodium channel functional expression by increasing its association with coat complex II and its exit from endoplasmic reticulum. *J. Biol. Chem.* **287,** 19255–19265 CrossRef Medline
42. Buck, T. M., Plavchak, L., Roy, A., Donnelly, B. F., Kashlan, O. B., Kleyman, T. R., Subramanya, A. R., and Brodsky, J. L. (2013) The Lhs1/GRP170 chaperones facilitate the endoplasmic reticulum-associated degradation of the epithelial sodium channel. *J. Biol. Chem.* **288,** 18366–18380 CrossRef Medline
43. Chanoux, R. A., Shubin, C. B., Robay, A., Suaud, L., and Rubenstein, R. C. (2013) Hsc70 negatively regulates epithelial sodium channel trafficking at multiple sites in epithelial cells. *Am. J. Physiol. Cell Physiol.* **305,** C776–C787 CrossRef Medline
44. Grumbach, Y., Bikard, Y., Suaud, L., Chanoux, R. A., and Rubenstein, R. C. (2014) ERp29 regulates epithelial sodium channel functional expression by promoting channel cleavage. *Am. J. Physiol. Cell Physiol.* **307,** C701–C709 CrossRef Medline
45. Buck, T. M., and Brodsky, J. L. (2018) Epithelial sodium channel biogenesis and quality control in the early secretory pathway. *Curr. Opin. Nephrol. Hypertens.* **27,** 364–372 CrossRef Medline
46. Devarajan, A., Shih, D., and Reddy, S. T. (2014) Inflammation, infection, cancer and all that: the role of paraoxonases. *Adv. Exp. Med. Biol.* **824,** 33–41 CrossRef Medline
47. Précourt, L. P., Amre, D., Denis, M. C., Lavoie, J. C., Delvin, E., Seidman, E., and Levy, E. (2011) The three-gene paraoxonase family: physiologic roles, actions and regulation. *Atherosclerosis* **214,** 20–36 CrossRef Medline
48. Draganov, D. I., Teiber, J. F., Speelman, A., Osawa, Y., Sunahara, R., and La Du, B. N. (2005) Human paraoxonases (PON1, PON2, and PON3) are lactonases with overlapping and distinct substrate specificities. *J. Lipid Res.* **46,** 1239–1247 CrossRef Medline
49. Ng, C. J., Shih, D. M., Hama, S. Y., Villa, N., Navab, M., and Reddy, S. T. (2005) The paraoxonase gene family and atherosclerosis. *Free Radic. Biol. Med.* **38,** 153–163 CrossRef Medline
50. Harel, M., Aharoni, A., Gaidukov, L., Brumshtein, B., Khersonsky, O., Meged, R., Dvir, H., Ravelli, R. B., McCarthy, A., Toker, L., Silman, I., Sussman, J. L., and Tawfik, D. S. (2004) Structure and evolution of the

serum paraoxonase family of detoxifying and anti-atherosclerotic enzymes. *Nat. Struct. Mol. Biol.* **11,** 412–419 CrossRef Medline
51. Mackness, M. I., Mackness, B., Durrington, P. N., Connelly, P. W., and Hegele, R. A. (1996) Paraoxonase: biochemistry, genetics and relationship to plasma lipoproteins. *Curr. Opin. Lipidol.* **7,** 69–76 CrossRef Medline
52. Draganov, D. I., Stetson, P. L., Watson, C. E., Billecke, S. S., and La Du, B. N. (2000) Rabbit serum paraoxonase 3 (PON3) is a high density lipoprotein-associated lactonase and protects low density lipoprotein against oxidation. *J. Biol. Chem.* **275,** 33435–33442 CrossRef Medline
53. Ng, C. J., Wadleigh, D. J., Gangopadhyay, A., Hama, S., Grijalva, V. R., Navab, M., Fogelman, A. M., and Reddy, S. T. (2001) Paraoxonase-2 is a ubiquitously expressed protein with antioxidant properties and is capable of preventing cell-mediated oxidative modification of low density lipoprotein. *J. Biol. Chem.* **276,** 44444–44449 CrossRef Medline
54. Marsillach, J., Mackness, B., Mackness, M., Riu, F., Beltrán, R., Joven, J., and Camps, J. (2008) Immunohistochemical analysis of paraoxonases-1, 2, and 3 expression in normal mouse tissues. *Free Radic. Biol. Med.* **45,** 146–157 CrossRef Medline
55. Chelur, D. S., Ernstrom, G. G., Goodman, M. B., Yao, C. A., Chen, L., O'Hagan, R., Chalfie, M. (2002) The mechanosensory protein MEC-6 is a subunit of the *C. elegans* touch-cell degenerin channel. *Nature* **420,** 669–673 CrossRef Medline
56. Chen, Y., Bharill, S., Altun, Z., O'Hagan, R., Coblitz, B., Isacoff, E. Y., and Chalfie, M. (2016) *Caenorhabditis elegans* paraoxonase-like proteins control the functional expression of DEG/ENaC mechanosensory proteins. *Mol. Biol. Cell* **27,** 1272–1285 CrossRef Medline
57. Shi, S., Buck, T. M., Kinlough, C. L., Marciszyn, A. L., Hughey, R. P., Chalfie, M., Brodsky, J. L., and Kleyman, T. R. (2017) Regulation of the epithelial $Na^+$ channel by paraoxonase-2. *J. Biol. Chem.* **292,** 15927–15938 CrossRef Medline
58. Gamliel-Lazarovich, A., Abassi, Z., Khatib, S., Tavori, H., Vaya, J., Aviram, M., and Keidar, S. (2012) Paraoxonase1 deficiency in mice is associated with hypotension and increased levels of 5,6-epoxyeicosatrienoic acid. *Atherosclerosis* **222,** 92–98 CrossRef Medline
59. Yang, Y., Zhang, Y., Cuevas, S., Villar, V. A., Escano, C., D Asico, L., Yu, P., Grandy, D. K., Felder, R. A., Armando, I., and Jose, P. A. (2012) Paraoxonase 2 decreases renal reactive oxygen species production, lowers blood pressure, and mediates dopamine D2 receptor-induced inhibition of NADPH oxidase. *Free Radic. Biol. Med.* **53,** 437–446 CrossRef Medline
60. Chen, L., Lee, J. W., Chou, C. L., Nair, A. V., Battistone, M. A., Păunescu, T. G., Merkulova, M., Breton, S., Verlander, J. W., Wall, S. M., Brown, D., Burg, M. B., and Knepper, M. A. (2017) Transcriptomes of major renal collecting duct cell types in mouse identified by single-cell RNA-seq. *Proc. Natl. Acad. Sci. U.S.A.* **114,** E9989–E9998 CrossRef Medline
61. Lee, J. W., Chou, C. L., and Knepper, M. A. (2015) Deep sequencing in microdissected renal tubules identifies nephron segment-specific transcriptomes. *J. Am. Soc. Nephrol.* **26,** 2669–2677 CrossRef Medline
62. Plotkin, M. D., Kaplan, M. R., Verlander, J. W., Lee, W. S., Brown, D., Poch, E., Gullans, S. R., and Hebert, S. C. (1996) Localization of the thiazide sensitive Na-Cl cotransporter, rTSC1 in the rat kidney. *Kidney Int.* **50,** 174–183 CrossRef Medline
63. Debonneville, C., Flores, S. Y., Kamynina, E., Plant, P. J., Tauxe, C., Thomas, M. A., Münster, C., Chraïbi, A., Pratt, J. H., Horisberger, J. D., Pearce, D., Loffing, J., and Staub, O. (2001) Phosphorylation of Nedd4-2 by Sgk1 regulates epithelial $Na^+$ channel cell surface expression. *EMBO J.* **20,** 7052–7059 CrossRef Medline
64. Taylor, A. N., McIntosh, J. E., and Bourdeau, J. E. (1982) Immunocytochemical localization of vitamin D-dependent calcium-binding protein in renal tubules of rabbit, rat, and chick. *Kidney Int.* **21,** 765–773 CrossRef Medline
65. Loffing, J., Loffing-Cueni, D., Valderrabano, V., Kläusli, L., Hebert, S. C., Rossier, B. C., Hoenderop, J. G., Bindels, R. J., and Kaissling, B. (2001) Distribution of transcellular calcium and sodium transport pathways along mouse distal nephron. *Am. J. Physiol. Renal Physiol.* **281,** F1021–F1027 CrossRef Medline
66. Fushimi, K., Uchida, S., Hara, Y., Hirata, Y., Marumo, F., and Sasaki, S. (1993) Cloning and expression of apical membrane water channel of rat kidney collecting tubule. *Nature* **361,** 549–552 CrossRef Medline
67. Miller, R. L., Zhang, P., Smith, M., Beaulieu, V., Paunescu, T. G., Brown, D., Breton, S., and Nelson, R. D. (2005) V-ATPase B1-subunit promoter drives expression of EGFP in intercalated cells of kidney, clear cells of epididymis and airway cells of lung in transgenic mice. *Am. J. Physiol. Cell Physiol.* **288,** C1134–C1144 CrossRef Medline
68. Bens, M., Vallet, V., Cluzeaud, F., Pascual-Letallec, L., Kahn, A., Rafestin-Oblin, M. E., Rossier, B. C., and Vandewalle, A. (1999) Corticosteroid-dependent sodium transport in a novel immortalized mouse collecting duct principal cell line. *J. Am. Soc. Nephrol.* **10,** 923–934 Medline
69. Carattino, M. D., Hill, W. G., and Kleyman, T. R. (2003) Arachidonic acid regulates surface expression of epithelial sodium channels. *J. Biol. Chem.* **278,** 36202–36213 CrossRef Medline
70. Shi, S., Carattino, M. D., Hughey, R. P., and Kleyman, T. R. (2013) ENaC regulation by proteases and shear stress. *Curr. Mol. Pharmacol.* **6,** 28–34 CrossRef Medline
71. Kleyman, T. R., Kashlan, O. B., and Hughey, R. P. (2018) Epithelial $Na^+$ channel regulation by extracellular and intracellular factors. *Annu. Rev. Physiol.* **80,** 263–281 CrossRef Medline
72. Carattino, M. D., Sheng, S., Bruns, J. B., Pilewski, J. M., Hughey, R. P., and Kleyman, T. R. (2006) The epithelial $Na^+$ channel is inhibited by a peptide derived from proteolytic processing of its $\alpha$ subunit. *J. Biol. Chem.* **281,** 18901–18907 CrossRef Medline
73. Hughey, R. P., Bruns, J. B., Kinlough, C. L., Harkleroad, K. L., Tong, Q., Carattino, M. D., Johnson, J. P., Stockand, J. D., and Kleyman, T. R. (2004) Epithelial sodium channels are activated by furin-dependent proteolysis. *J. Biol. Chem.* **279,** 18111–18114 CrossRef Medline
74. Bruns, J. B., Carattino, M. D., Sheng, S., Maarouf, A. B., Weisz, O. A., Pilewski, J. M., Hughey, R. P., and Kleyman, T. R. (2007) Epithelial $Na^+$ channels are fully activated by furin- and prostasin-dependent release of an inhibitory peptide from the $\gamma$-subunit. *J. Biol. Chem.* **282,** 6153–6160 CrossRef Medline
75. Passero, C. J., Mueller, G. M., Rondon-Berrios, H., Tofovic, S. P., Hughey, R. P., and Kleyman, T. R. (2008) Plasmin activates epithelial $Na^+$ channels by cleaving the $\gamma$ subunit. *J. Biol. Chem.* **283,** 36586–36591 CrossRef Medline
76. Passero, C. J., Mueller, G. M., Myerburg, M. M., Carattino, M. D., Hughey, R. P., and Kleyman, T. R. (2012) TMPRSS4-dependent activation of the epithelial sodium channel requires cleavage of the $\gamma$-subunit distal to the furin cleavage site. *Am. J. Physiol. Renal Physiol.* **302,** F1–F8 CrossRef Medline
77. Kellenberger, S., Gautschi, I., and Schild, L. (2002) An external site controls closing of the epithelial $Na^+$ channel ENaC. *J. Physiol.* **543,** 413–424 CrossRef Medline
78. Snyder, P. M., Olson, D. R., and Bucher, D. B. (1999) A pore segment in DEG/ENaC $Na^+$ channels. *J. Biol. Chem.* **274,** 28484–28490 CrossRef Medline
79. Meyer, W. K., Jamison, J., Richter, R., Woods, S. E., Partha, R., Kowalczyk, A., Kronk, C., Chikina, M., Bonde, R. K., Crocker, D. E., Gaspard, J., Lanyon, J. M., Marsillach, J., Furlong, C. E., and Clark, N. L. (2018) Ancient convergent losses of Paraoxonase 1 yield potential risks for modern marine mammals. *Science* **361,** 591–594 CrossRef Medline
80. Shih, D. M., Xia, Y. R., Yu, J. M., and Lusis, A. J. (2010) Temporal and tissue-specific patterns of Pon3 expression in mouse: in situ hybridization analysis. *Adv. Exp. Med. Biol.* **660,** 73–87 CrossRef Medline
81. Shih, D. M., Yu, J. M., Vergnes, L., Dali-Youcef, N., Champion, M. D., Devarajan, A., Zhang, P., Castellani, L. W., Brindley, D. N., Jamey, C., Auwerx, J., Reddy, S. T., Ford, D. A., Reue, K., and Lusis, A. J. (2015) PON3 knockout mice are susceptible to obesity, gallstone formation, and atherosclerosis. *FASEB J.* **29,** 1185–1197 CrossRef Medline
82. Wiemuth, D., Sahin, H., Falkenburger, B. H., Lefèvre, C. M., Wasmuth, H. E., and Gründer, S. (2012) BASIC: a bile acid-sensitive ion channel highly expressed in bile ducts. *FASEB J.* **26,** 4122–4130 CrossRef Medline
83. Wiemuth, D., Sahin, H., Lefèvre, C. M., Wasmuth, H. E., and Gründer, S. (2013) Strong activation of bile acid-sensitive ion channel (BASIC) by ursodeoxycholic acid. *Channels* **7,** 38–42 CrossRef Medline
84. Li, Q., Kresge, C., Bugde, A., Lamphere, M., Park, J. Y., and Feranchak, A. P. (2016) Regulation of mechanosensitive biliary epithelial transport by the epithelial $Na^+$ channel. *Hepatology* **63,** 538–549 CrossRef Medline

85. Wang, X. P., Im, S. J., Balchak, D. M., Montalbetti, N., Carattino, M. D., Ray, E. C., and Kashlan, O. B. (2019) Murine epithelial sodium ($Na^+$) channel regulation by biliary factors. *J. Biol. Chem.* **294,** 10182–10193 CrossRef Medline
86. Loffing, J., Pietri, L., Aregger, F., Bloch-Faure, M., Ziegler, U., Meneton, P., Rossier, B. C., and Kaissling, B. (2000) Differential subcellular localization of ENaC subunits in mouse kidney in response to high- and low-Na diets. *Am. J. Physiol. Renal Physiol.* **279,** F252–F258 CrossRef Medline
87. Mick, V. E., Itani, O. A., Loftus, R. W., Husted, R. F., Schmidt, T. J., and Thomas, C. P. (2001) The $\alpha$-subunit of the epithelial sodium channel is an aldosterone-induced transcript in mammalian collecting ducts, and this transcriptional response is mediated via distinct *cis*-elements in the 5′-flanking region of the gene. *Mol. Endocrinol.* **15,** 575–588 CrossRef Medline
88. Loffing, J., Zecevic, M., Féraille, E., Kaissling, B., Asher, C., Rossier, B. C., Firestone, G. L., Pearce, D., and Verrey, F. (2001) Aldosterone induces rapid apical translocation of ENaC in early portion of renal collecting system: possible role of SGK. *Am. J. Physiol. Renal Physiol.* **280,** F675–F682 CrossRef Medline
89. Náray-Fejes-Tóth, A., and Fejes-Tóth, G. (2000) The sgk, an aldosterone-induced gene in mineralocorticoid target cells, regulates the epithelial sodium channel. *Kidney Int.* **57,** 1290–1294 CrossRef Medline
90. Blazer-Yost, B. L., Liu, X., and Helman, S. I. (1998) Hormonal regulation of ENaCs: insulin and aldosterone. *Am. J. Physiol.* **274,** C1373–C1379 CrossRef Medline
91. Gründer, S., and Rossier, B. C. (1997) A reappraisal of aldosterone effects on the kidney: new insights provided by epithelial sodium channel cloning. *Curr. Opin. Nephrol. Hypertens.* **6,** 35–39 CrossRef Medline
92. Denault, D. L., Fejes-Tóth, G., and Náray-Fejes-Tóth, A. (1996) Aldosterone regulation of sodium channel $\gamma$-subunit mRNA in cortical collecting duct cells. *Am. J. Physiol.* **271,** C423–C428 CrossRef Medline
93. Schafer, J. A., and Hawk, C. T. (1992) Regulation of $Na^+$ channels in the cortical collecting duct by AVP and mineralocorticoids [editorial]. *Kidney Int.* **41,** 255–268 CrossRef Medline
94. Rubera, I., Loffing, J., Palmer, L. G., Frindt, G., Fowler-Jaeger, N., Sauter, D., Carroll, T., McMahon, A., Hummler, E., and Rossier, B. C. (2003) Collecting duct-specific gene inactivation of $\alpha$ENaC in the mouse kidney does not impair sodium and potassium balance. *J. Clin. Invest.* **112,** 554–565 CrossRef Medline
95. Christensen, B. M., Perrier, R., Wang, Q., Zuber, A. M., Maillard, M., Mordasini, D., Malsure, S., Ronzaud, C., Stehle, J. C., Rossier, B. C., and Hummler, E. (2010) Sodium and potassium balance depends on $\alpha$ENaC expression in connecting tubule. *J. Am. Soc. Nephrol.* **21,** 1942–1951 CrossRef Medline
96. Nesterov, V., Dahlmann, A., Krueger, B., Bertog, M., Loffing, J., and Korbmacher, C. (2012) Aldosterone-dependent and -independent regulation of the epithelial sodium channel (ENaC) in mouse distal nephron. *Am. J. Physiol. Renal Physiol.* **303,** F1289–F1299 CrossRef Medline
97. Frindt, G., and Palmer, L. G. (2004) Na channels in the rat connecting tubule. *Am. J. Physiol. Renal Physiol.* **286,** F669–F674 CrossRef Medline
98. Snyder, P. M., Price, M. P., McDonald, F. J., Adams, C. M., Volk, K. A., Zeiher, B. G., Stokes, J. B., and Welsh, M. J. (1995) Mechanism by which Liddle's syndrome mutations increase activity of a human epithelial $Na^+$ channel. *Cell* **83,** 969–978 CrossRef Medline
99. Fang, X., Fukuda, N., Barbry, P., Sartori, C., Verkman, A. S., and Matthay, M. A. (2002) Novel role for CFTR in fluid absorption from the distal airspaces of the lung. *J. Gen. Physiol.* **119,** 199–207 CrossRef Medline
100. Mall, M. A., Button, B., Johannesson, B., Zhou, Z., Livraghi, A., Caldwell, R. A., Schubert, S. C., Schultz, C., O'Neal, W. K., Pradervand, S., Hummler, E., Rossier, B. C., Grubb, B. R., and Boucher, R. C. (2010) Airway surface liquid volume regulation determines different airway phenotypes in Liddle compared with $\beta$ENaC-overexpressing mice. *J. Biol. Chem.* **285,** 26945–26955 CrossRef Medline
101. Rauh, R., Diakov, A., Tzschoppe, A., Korbmacher, J., Azad, A. K., Cuppens, H., Cassiman, J. J., Dötsch, J., Sticht, H., and Korbmacher, C. (2010) A mutation of the epithelial sodium channel associated with atypical cystic fibrosis increases channel open probability and reduces $Na^+$ self inhibition. *J. Physiol.* **588,** 1211–1225 CrossRef Medline
102. You, H., Ge, Y., Zhang, J., Cao, Y., Xing, J., Su, D., Huang, Y., Li, M., Qu, S., Sun, F., and Liang, X. (2017) Derlin-1 promotes ubiquitylation and degradation of the epithelial $Na^+$ channel, ENaC. *J. Cell Sci.* **130,** 1027–1036 Medline
103. Grifoni, S. C., McKey, S. E., and Drummond, H. A. (2008) Hsc70 regulates cell surface ASIC2 expression and vascular smooth muscle cell migration. *Am. J. Physiol. Heart Circ. Physiol.* **294,** H2022–H2030 CrossRef Medline
104. Joyce-Brady, M., Jean, J. C., and Hughey, R. P. (2001) $\gamma$-Glutamyltransferase and its isoform mediate an endoplasmic reticulum stress response. *J. Biol. Chem.* **276,** 9468–9477 CrossRef Medline
105. Klemens, C. A., Edinger, R. S., Kightlinger, L., Liu, X., and Butterworth, M. B. (2017) Ankyrin G expression regulates apical delivery of the epithelial sodium channel (ENaC). *J. Biol. Chem.* **292,** 375–385 CrossRef Medline
106. Kashlan, O. B., Kinlough, C. L., Myerburg, M. M., Shi, S., Chen, J., Blobner, B. M., Buck, T. M., Brodsky, J. L., Hughey, R. P., and Kleyman, T. R. (2018) *N*-linked glycans are required on epithelial $Na^+$ channel subunits for maturation and surface expression. *Am. J. Physiol. Renal Physiol.* **314,** F483–F492 CrossRef Medline
107. Hughey, R. P., Altman, R. A., Wells, W. J., and Curto, K. A. (1986) Evidence for stable homodimers and heterodimers of $\gamma$-glutamyltranspeptidase subunits under protein-denaturing conditions. *Biochim. Biophys. Acta* **874,** 150–159 CrossRef Medline